ACS Photonics

Article

pubs.acs.org/journal/apchd5

Solution-Processed, High-Speed, and High-Quantum-Efficiency Quantum Dot Infrared Photodetectors

Jianbo Gao,[†,‡] Son C. Nguyen,[†] Noah D. Bronstein,[†] and A. Paul Alivisatos*[,†,‡,§,⊥]

[†]Department of Chemistry and [‡]Department of Materials Science and Engineering, University of California, Berkeley, California 94720, United States

[§]Materials Sciences Division, Lawrence Berkeley National Laboratory, Berkeley, California 94720, United States

[⊥]Kavli Energy Nanosciences Institute, University of California, Berkeley, and Lawrence Berkeley National Lab, Berkeley, California 94720, United States

Supporting Information

ABSTRACT: For over a decade, much effort has been focused on passivation of the high density of localized electronic trap states in colloidal semiconductor quantum dots (QDs), which lead to reduced performance in solar cell, light-emitting diode, laser, and photoconductor applications. However, here we take advantage of the naturally occurring high density of trap states to demonstrate solution-processed high-speed PbSe quantum dot near-infrared photodetectors. Carrier transport dynamics studies reveal multiple trapping and release transport dynamics in band tail states. A sandwich microstrip transmission line photodetector utilizing these QD films was fabricated to achieve high performance by allowing carriers to be swept to the electrodes before they fall into the band tail states. This device demonstrates external quantum efficiency, responsivity, and response time (full width at half-maximum) of 54%, 0.36 A/W, and 74 ps, respectively.

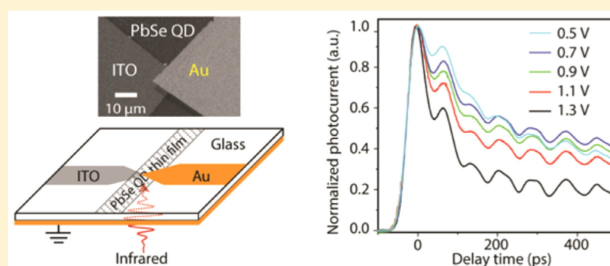

KEYWORDS: *quantum dots, photodetector, high speed, quantum efficiency, transport, trap states, multiple trapping and release*

HIGH-SPEED IR PHOTODETECTORS: BACKGROUND AND CHALLENGES

In a high-speed photodetector, pulsed illumination of a semiconductor transiently increases the population of mobile charges above the steady-state thermal background level. There are subtle aspects of design that are required to take advantage of this transient population in creating an effective high-speed detector. Solution-processing, flexibility, and complementary metal−oxide−semiconductor (CMOS) integrability are desirable for next-generation high-speed infrared (IR) photodetectors.[1,2] A notable example is the graphene-based high-speed IR photodetector. Although the ~10's ps carrier lifetime of band-to-band direct recombination (depicted in Figure 1) affords a fast response time in graphene devices,[3] the small carrier generation area and low optical absorption result in low quantum efficiency and responsivity of the detector.[4] In contrast, higher absorption could be achieved with colloidal quantum dots (QDs). These colloidal QDs can readily be deposited using solution processing on rigid or flexible insulating, crystalline, or amorphous substrates. Very high mobility, such as occurs in a pristine material, enables rapid sweeping of the charges across the device. This rapid sweeping mechanism, as shown in Figure 1, has been successfully utilized to fabricate high-speed IR photodetectors made from InGaAs or InSb;[5,6] however, the above bulk semiconductor devices require high temperature and high vacuum during fabrication, in addition to strict lattice constant match, limiting the ease of integration with other semiconductor devices. Lead chalcogenide QDs (PbSe, PbS, PbTe) can be electronically coupled in densely packed thin films through the use of short-chain acids,[7] thiols,[8] or ammonium thiocyanate.[9] This coupling results in field-effect mobility close to 1 $cm^2/(V\ s)$.[10] Thus, in well-designed devices, it is possible to sweep the carrier from one electrode to another under a high electric field before they are trapped. For example, a device with a mobility of 1 $cm^2/(V\ s)$ with a 100 nm transit length and a field in the range of 10^6 V/cm should collect the band-edge electrons in around 10 ps if the attached circuit can respond quickly enough. Deep traps

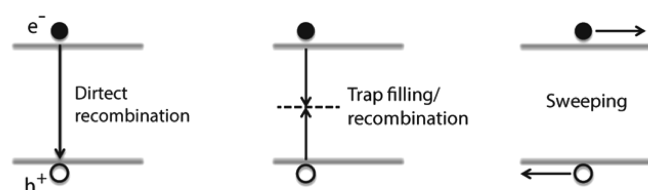

Figure 1. Three operation mechanisms of high-speed photodetectors leading to high-speed response: direct recombination of electron and hole, trap filling through recombination centers, and carrier sweeping.

Received: March 26, 2016
Published: June 21, 2016

© 2016 American Chemical Society

DOI: 10.1021/acsphotonics.6b00211
ACS Photonics 2016, 3, 1217−1222

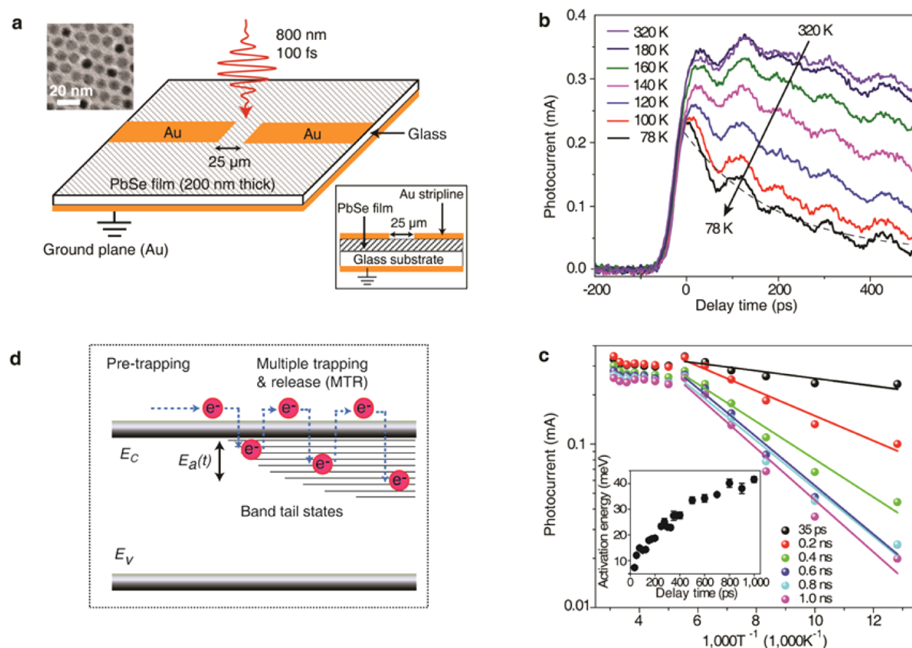

Figure 2. High-speed QD photodetector using a coplanar microstrip transmission line structure. (a) Scheme of the photodetector structure (middle), TEM image of 8 nm PbSe QDs (top left inset) used, and the device cross-section (bottom right inset). (b) Transient photocurrent traces under various temperatures from 78 to 320 K for a PbSe QD thin film treated with ethanedithiol. The laser fluence is 8.3 mW/cm^2, and the electric field is 8×10^3 V/cm. The dashed line is a representative exponential fit of a photocurrent at 78 K. The ringing effect is due to impedance mismatch of the photoconductive devices, the coaxial cables, and the connectors. (c) Arrhenius plots of the log photocurrent at various delay times in part b as a function of $1000/T$. The inset is the extracted activation energy, $E_a(t)$, for carrier escape from the band tail states as a function of delay time. (d) Scheme of multiple trap and release transport dynamics in the band tail states, illustrating that activation $E_a(t)$ increases with longer delay time after photoexcitation, as the charges fall into deeper traps over time. A similar transport dynamics model is also applied to the hole carrier in the band tail states.

with lower mobility can paradoxically improve performance, however, because they can act as recombination centers that suppress dark current, as shown in Figure 1. This helps to explain why so much work in high-speed photodetectors has involved ion implantation to generate defects in thin-film InGaAs,[11] GaAs,[12,13] GaP,[14] and other such high-quality semiconductors. The advent of the ability to tailor-make quantum dots offers a new set of opportunities for high-speed photodetector design. Each dot represents a small region of high quality, surrounded by an interface that possesses defects that can be modulated through surface modification. QDs usually have a high density of in-gap defect states due to their large surface-to-volume ratio. A simple estimate suggests that one effective defect state in a 3 nm diameter QD will result in a trapping time of a couple of picoseconds (see SI). This offers significant advantages for lowering dark current, but also restricts the mobility. This paper aims to explore this limit, specifically in the examination of high-speed detectors. Design considerations here slightly differ from those of time-integrating high-gain photodetectors with much slower response times in the range of microseconds,[15,16] which are operated under steady-state illumination conditions. In steady-state devices, gain is achieved through the reinjection of high-mobility holes, which circulate to maintain charge neutrality as long as there are long-lived low-mobility electrons in deep trap states. In high-speed photodetectors, on the other hand, illumination is via pulsed photons, and only the directly photogenerated charges participate in the observed current transient, with no carrier reinjection through electrodes.

In this report, we use a room-temperature solution-processed PbSe QD film as a model system. We first use an Auston photoconductive photodetector with a coplanar microstrip transmission line structure to investigate the carrier transport dynamics.[17−20] The device geometry is similar to that used previously for slow-speed and high-responsivity PbS QD photodetectors,[16] but we incorporate the photodetector as an integral component of a high-speed transmission line with a gold electrode in a split microstrip line.[21] Therefore, the electrode capacitance and inductance are distributed in the form of a transmission line, leaving only a small capacitance associated with the active material region of the photoconductor (i.e., the spacing) to affect the speed of response.[20] We discovered that carriers rapidly fall into trap states upon photoexcitation followed by multiple trapping and release (MTR) transport in the band tail states, characterized by time-dependent shallow trap levels, carrier escape frequency, and carrier capture cross-section. Next, we use the lessons learned in the Auston-switch device to build a faster and more efficient high-speed IR photodetector, demonstrating a ~50% EQE, a responsivity of 0.36 A/W, and a response time fwhm of 74 ps. We were unable to create a faster device due to the system response time limited by the bandwidth of the sampling oscilloscope, coaxial cable, and connectors.

■ COPLANAR MICROSTRIP TRANSMISSION LINE HIGH-SPEED PHOTODETECTOR TO CHARACTERIZE CARRIER TRANSPORT DYNAMICS

Figure 2a shows the Auston-switch photodetector structure with coplanar microstrip transmission line electrodes. A detailed description of the QD synthesis and photodetector fabrication can be found in the Materials and Methods section of the SI. Briefly, a 200 nm thick film of 8 nm diameter PbSe

DOI: 10.1021/acsphotonics.6b00211
ACS Photonics 2016, 3, 1217−1222

QDs with a first absorption peak at 2100 nm is prepared by a hand-dipping layer-by-layer method on a glass substrate with the QD solution with 1 mM concentration ethanedithiol (EDT) inside a nitrogen-filled glovebox. The absorption spectra of the PbSe QDs in hexane solvent and the crack-free PbSe QD film with a roughness of 3.9 nm are shown in Figures S1−S3. The top Au coplanar electrodes with 25 μm spacing and the Au ground plane beneath the glass substrate are thermally evaporated under vacuum. Therefore, the microstrip transmission line design, consisting of top and bottom Au thin films with a glass substrate and active PbSe thin film, allows high-speed signal transmission. One side of the electrode is biased with a power supply, and the other side is connected to a sampling oscilloscope through a coaxial cable. The whole device was encapsulated in a custom air-free holder and mounted into an optical cryostat. The device's fast photocurrent response is characterized by illumination with a 1 KHz repetition rate, 800 nm wavelength laser with 100 fs pulses onto the active PbSe QD film to generate photocurrent, which is collected by a 20 GHz sampling oscilloscope. The excitation photon energy is $2.6E_g$ of the QD band gap (E_g), well below the threshold $3E_g$ that may be associated with phenomena of multiple exciton generation. The transient photocurrent has a rise time of 35 ps, resulting from the bandwidth of the sampling oscilloscope, coaxial cables, and connectors (as shown in Figure S4). After the fast rise, the photocurrent has a fast decay in hundreds of picoseconds and a slow decay extending to a couple of nanoseconds, which may be due to the decay of carriers in the midgap states.[22] The fast decay is of interest to us, because it is a characteristic of the device response time. Figure 2b shows typical transient photocurrent traces at 8.3 mW/cm^2 fluence and 20 V bias under various temperatures in the temporal range of 0 to 500 ps. In this study the photon flux is below the threshold for more than one photon to be absorbed per dot. (The photocurrent decay trace extended to time scales of nanoseconds is shown in Figure S5 with biexponential decay fitting.)

Figure 2b shows the photocurrent decay as a function of temperature. The photocurrent decays faster at lower temperatures, indicating thermally activated carrier transport behavior. Upon photoexcitation, the carriers thermalize toward the band edge within a couple of picoseconds.[23] This thermalization process is not resolved in our experiment due to limited temporal resolution. The carriers then fall into trap states, including band tail states, deep traps, or transport to other dots, or undergo electron−hole recombination; other trapping mechanisms are possible via surface exciton trapping, as observed by Sewall et al.[24] When the carriers fall into the band tail with an energy width comparable to k_BT, we expect that the carrier can occasionally gain enough thermal energy to be released back from the band tail to the band, further contributing to the photocurrent. We exclude the bolometric effect due to laser excitation that results in a negligible temperature increase of 0.13 K (see detailed calculation in SI). The rate of this release process should decrease exponentially with the energy depth of the traps as the carriers fall deeper into the band tail, leading to a broad distribution of release times and thus a non-monoexponential decay of the photocurrent in time. This multiple trapping and release transport dynamic[25−28] (illustrated in Figure 2d) shows much faster photocurrent decay with lower temperatures, as seen in Figure 2b. At a low temperature, the trapped carriers have less chance to escape from the trap states, resulting in faster photocurrent decay at short times. Similar behavior was observed in other low-mobility systems such as organic semiconductor polymers,[29,30] amorphous semiconductors,[31] and C_{60}.[32] To determine the activation energy required to release the carrier from the band tail, $E_a(t)$, we plot the Arrhenius relation of the photocurrent at various delay times (Figure 2c). The Arrhenius fitting (Figure 2c, inset) clearly shows that the trap depth $E_a(t)$ increases from ∼5 meV at 35 ps to 32 meV at 600 ps and then continues up to 40 meV at 1 ns. The observed band tail depth is consistent with other reported values characterized by voltage−current measurements.[33,34]

We have characterized the band tail properties by determining the capture cross-section and detrapping rate, which are directly related to the device response time. More importantly, they are desirable parameters that can be uniquely characterized by the transient photocurrent technique. According to MTR dynamics, the detrapping rate or the attempt-to-escape frequency of the carrier, ν_0, can be obtained by the following relation:[25,28]

$$\nu_0 = \exp(E_a(t)/k_BT)/t \tag{1}$$

,where $E_a(t)$ is the activation energy, k_B is the Boltzmann constant, T is the temperature, and ν_0 is the attempt-to-escape frequency. Equation 1 assumes that carrier release is a thermally activated process. By fitting the $E_a(t)$ at various delay times from 35 to 400 ps to eq 1, the attempt-to-escape frequency obtained is 2.6×10^{10}/s. (see Figure S6). The capture cross-section of the trap states representing the probability of the trap capturing the carriers, δ_n, can be calculated from the following equation:[16]

$$\delta_n = \nu_0/k_BT\ g(E)\ \nu_{th} \tag{2}$$

,where $g(E)$ is the density of states and ν_{th} is the carrier thermal velocity of 10^7 cm/s. In particular, at 78 K, where most carriers fall into trap states without thermal release to contribute to current, we take the density of states in the range of $\sim 10^{19}$ cm^{-3} eV^{-1} from literature;[35] the extracted capture cross-section value is 4.3×10^{-13} cm^2. This is equivalent to a dot size of 6.6 nm, which is close to the studied PbSe QD dot size of 8 nm. This indicates that at low temperature carriers are trapped in one dot and possibly captured at dot surface defect states, resulting in the fast response time of 202 ps. To the best of our knowledge, these are the first reported experimental values for carrier detrapping rates and trap-capture cross-sections of PbSe QD films. By obtaining photocurrent dependence with laser fluence measurements, we extract the density of trap states of 10^{17}/cm^3 (see Figure S7), consistent with previous studies of EDT treatment of PbSe dots.[33,34] As illustrated in Figure S7, the photocurrent decays faster with increasing laser fluence above 50 μW, strongly suggesting an Auger recombination mechanism. This further argues that the decay dynamics dependence on temperature is due to a trapping mechanism under the low laser fluence of 8.3 mW/cm^2 (40 μW) in this study and not due to Auger recombination.

By utilizing the trapping−filling mechanism into trap states at the lowest tested temperature of 78 K, the Auston-switch photodetector studied above has the best performance with an external quantum efficiency (EQE), responsivity, and response time fwhm of 10^{-3}%, 4.0×10^{-5} A/W, and 202 ps, respectively (see calculations in SI). The trap filling mechanism results in a fast photocurrent decay time, but at the cost of poor device performance, mainly due to the poor carrier collection efficiency during transport. In order to improve the EQE and

DOI: 10.1021/acsphotonics.6b00211
ACS Photonics 2016, 3, 1217−1222

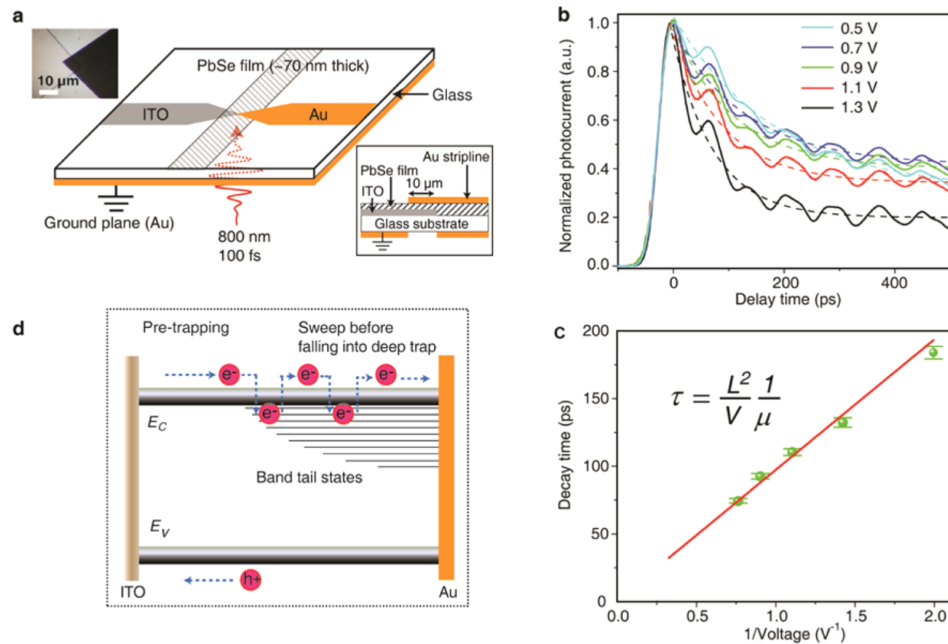

Figure 3. High-speed, high-efficiency QD photodetector using sandwich microstrip transmission line structure. (a) Scheme of the device with a PbSe QD thin film sandwiched between a bottom ITO electrode and a top Au electrode. Actual image of overlapped area (~100 μm^2) of the two electrodes (top left inset); device cross-section (bottom right inset). (b) Transient photocurrent traces under various biases at room temperature and a laser fluence of 0.42 mW/cm^2. Dashed lines are fitted single-exponential decays of the photocurrents. (c) The photocurrent decay lifetimes are inversely proportional to the applied biases. (d) Schematic illustrating the proposed transport dynamics under the carrier sweeping transport mechanism.

Table 1. Key Parameters of Our High-Speed IR Photodetectors of QD-Based and Reported Graphene Devices[3]

photodetector structure	bias (V)	EQE (%)	responsivity (A/W)	fwhm (ps)	operating temperature	dark current density (mA/cm^2)
sandwich	1.3	54	0.36	74	room T	1.15×10^5
graphene	0	0.5	6.1×10^{-3}	<11	room T	0

responsivity while maintaining the fast response time under room-temperature operation condition, an additional device architecture is implemented in which the carriers are swept by a high electric field to the electrodes before they can fall into the deep trap states.

SANDWICH MICROSTRIP TRANSMISSION LINE PHOTODETECTOR WITH CARRIER SWEEPING MECHANISM

In the new photodetector architecture, a high electric field in the range of 1.9×10^5 V/cm (1.3 V/70 nm) sweeps out the carriers to the electrodes before they fall into the deeper trap states. This design can be achieved with a small electrode separated by a thin layer of PbSe QDs of 70 nm thickness, as illustrated in Figure 3a, where a PbSe QD film is dip-coated by hand on a prepatterned ITO microstrip line of 50 Ω impedance. The transparent contact of ITO allows laser illumination through the glass/ITO contact. The top Au stripline was thermally evaporated through a shadow mask onto the top surface of the PbSe QD film in such a manner that the overlap area with the bottom ITO contact was ~100 μm^2. The ITO side was biased with a power supply, and the Au side transmitted the signal directly to the sampling oscilloscope. Au is known to form an ohmic contact with PbSe QDs.[36] Using a parallel plate capacitor model, we estimated the circuit rise time constant to be 14 ps (detailed calculation in SI), which indicates that the measurement will still be limited by the system bandwidth of 35 ps. Figure 3b clearly shows that the photocurrent decays faster under higher bias: a 0.7 V bias results in a photocurrent decay time of 130 ps; increasing the bias to 1.3 V, the decay time hastens to 74 ps, nearly 3 times faster than the coplanar device. Faster decay below 74 ps and decay less than 20% of peak current are expected under higher bias; however, bias voltage above 1.3 V led to device breakdown. The faster decay under higher bias indicates that the carriers are swept to the electrodes by the electric field. With the carrier sweeping mechanism, the relationship between decay time and applied bias is governed by

$$\tau = \left(\frac{1}{\mu}\right)\left(\frac{L^2}{V}\right) \tag{3}$$

,where τ is the sweep time, μ is the majority carrier mobility of holes, L is the film thickness, and V is the bias voltage; we calculate the mobility from the slope of 0.26 cm^2/(V s), which is consistent with other reported values in the literature.[7,10] We further calculate the key parameters of the high-speed sandwich photodetectors. The calculated EQE is 54% and the responsivity is 0.36 A/W under 1.3 V bias, indicating significantly improved carrier extraction compared to a coplanar device (see calculations in SI). Without taking into account any optical loss due to reflection and absorption of the ITO, the above-calculated parameters may compensate for the weak absorption at longer wavelengths for IR photodetectors, while the characteristic excitation wavelength is 800 nm in our case. The quantum efficiency and responsivity improvement is due

DOI: 10.1021/acsphotonics.6b00211
ACS Photonics 2016, 3, 1217−1222

to enhanced carrier collection efficiency before electrons and holes recombine or fall into trap states. The calculated carrier drift length under 1.3 V bias is estimated as 50 nm, comparable to the PbSe QD film thickness of 70 nm, allowing about 70% of the carriers to be collected before they are trapped.

The key photodetector parameters are tabulated in Table 1, along with the most comparable nanostructured IR high-speed photodetector based on graphene.[1,3] The QD-based sandwich photodetector has superior EQE and responsivity. However, the dark current density for QD-based devices is quite high due to the ohmic contacts, on the order of $\sim 10^5$ mA/cm^2, as shown in Figure S8. This could be minimized by adding an electron- or a hole-blocking layer between electrodes and the PbSe QD films, as suggested by other studies.[37]

In conclusion, the high-speed photodetector can be operated via a trapping mechanism, but demonstrates inferior device performance due to poor carrier collection efficiency. On the other hand, using a carrier sweep mechanism, we have shown high-speed photodetectors with state-of-the-art performance with ~50% EQE, responsivity of 0.36 A/W, and response time fwhm of 74 ps at room temperature. This is realized by reconfiguring the device in a sandwich electrode geometry between Au and ITO with a small overlap area of 100 μm^2. The device operation mechanism and device architecture can be generally applied to other semiconductor QDs. In addition to superior device performance, the unique feature of solution processing and tunable absorption wavelength covering the near IR and IR range enable semiconductor QDs promising applications in optical communications, sensors, and surveillance.[38,39]

■ ASSOCIATED CONTENT

Ⓢ Supporting Information

The Supporting Information is available free of charge on the ACS Publications website at DOI: 10.1021/acsphotonics.6b00211.

Materials and Methods section (PDF)

■ AUTHOR INFORMATION

Corresponding Author

*E-mail: paul.alivisatos@berkeley.edu.

Author Contributions

J. Gao and S. C. Nguyen are equal contributors.

Notes

The authors declare no competing financial interest.

■ ACKNOWLEDGMENTS

This work is supported by the Physical Chemistry of Inorganic Nanostructures Program, KC3103, Office of Basic Energy Sciences of the United States Department of Energy, under Contract No. DE-AC02-05CH11231. We would also like to thank Danny Hellebusch for useful discussion.

■ REFERENCES

(1) Koppens, F. H. L.; Mueller, T.; Avouris, P.; Ferrari, A. C.; Vitiello, M. S.; Polini, M. Photodetectors Based on Graphene, other Two-dimensional Materials and Hybrid Systems. *Nat. Nanotechnol.* **2014**, *9*, 780–793.

(2) Novoselov, K. S.; Fal'ko, V. I.; Colombo, L.; Gellert, P. R.; Schwab, M. G.; Kim, K. A roadmap for Graphene. *Nature* **2012**, *490*, 192–200.

(3) Xia, F. N.; Mueller, T.; Lin, Y. M.; Valdes-Garcia, A.; Avouris, P. Ultrafast Graphene Photodetector. *Nat. Nanotechnol.* **2009**, *4*, 839–843.

(4) Bonaccorso, F.; Sun, Z.; Hasan, T.; Ferrari, A. C. Graphene Photonics and Optoelectronics. *Nat. Photonics* **2010**, *4*, 611–622.

(5) Kimukin, I.; Biyikli, N.; Kartaloglu, T.; Aytur, O.; Ozbay, E. High-speed InSb Photodetectors on GaAs for Mid-IR Applications. *IEEE J. Sel. Top. Quantum Electron.* **2004**, *10*, 766–770.

(6) Shimizu, N.; Watanabe, N.; Furuta, T.; Ishibashi, T. Electron Diffusivity in p-InGaAs Determined from the Pulse Response of InP/InGaAs Uni-traveling-carrier Photodiodes. *Appl. Phys. Lett.* **2000**, *76*, 1191–1193.

(7) Zarghami, M. H.; Liu, Y.; Gibbs, M.; Gebremichael, E.; Webster, C.; Law, M. p-Type PbSe and PbS Quantum Dot Solids Prepared with Short-Chain Acids and Diacids. *ACS Nano* **2010**, *4*, 2475–2485.

(8) Liu, Y.; Gibbs, M.; Puthussery, J.; Gaik, S.; Ihly, R.; Hillhouse, H. W.; Law, M. Dependence of Carrier Mobility on Nanocrystal Size and Ligand Length in PbSe Nanocrystal Solids. *Nano Lett.* **2010**, *10*, 1960–1969.

(9) Oh, S. J.; Berry, N. E.; Choi, J. H.; Gaulding, E. A.; Lin, H. F.; Paik, T.; Diroll, B. T.; Muramoto, S.; Murray, C. B.; Kagan, C. R. Designing High-Performance PbS and PbSe Nanocrystal Electronic Devices through Stepwise, Post-Synthesis, Colloidal Atomic Layer Deposition. *Nano Lett.* **2014**, *14*, 1559–1566.

(10) Hetsch, F.; Zhao, N.; Kershaw, S. V.; Rogach, A. L. Quantum Dot Field Effect Transistors. *Mater. Today* **2013**, *16*, 312–325.

(11) Baker, C.; Gregory, I. S.; Tribe, W. R.; Bradley, I. V.; Evans, M. J.; Linfield, E. H.; Missous, M. Highly Resistive Annealed Low-temperature-grown InGaAs with Sub-500 fs Carrier Lifetimes. *Appl. Phys. Lett.* **2004**, *85*, 4965–4967.

(12) Melloch, M. R.; Woodall, J. M.; Harmon, E. S.; Otsuka, N.; Pollak, F. H.; Nolte, D. D.; Feenstra, R. M.; Lutz, M. A. Low-Temperature-Grown III-V Materials. *Annu. Rev. Mater. Sci.* **1995**, *25*, 547–600.

(13) Gupta, S.; Whitaker, J. F.; Mourou, G. A. Ultrafast Carrier Dynamics in III-V-Semiconductors Grown by Molecular-Beam Epitaxy at Very Low Substrate Temperatures. *IEEE J. Quantum Electron.* **1992**, *28*, 2464–2472.

(14) Foyt, A. G.; Leonberger, F. J.; Williamson, R. C. Picosecond InP Optoelectronic Switches. *Appl. Phys. Lett.* **1982**, *40*, 447–449.

(15) Konstantatos, G.; Sargent, E. H. Colloidal Quantum Dot Photodetectors. *Infrared Phys. Technol.* **2011**, *54*, 278–282.

(16) Konstantatos, G.; Howard, I.; Fischer, A.; Hoogland, S.; Clifford, J.; Klem, E.; Levina, L.; Sargent, E. H. Ultrasensitive solution-cast quantum dot photodetectors. *Nature* **2006**, *442*, 180–183.

(17) Auston, D. H. Picosecond Optoelectronic Switching and Gating in Silicon. *Appl. Phys. Lett.* **1975**, *26*, 101–103.

(18) Johnson, A. M.; Glass, A. M.; Olson, D. H.; Simpson, W. M.; Harbison, J. P. High Quantum Efficiency Amorphous-Silicon Photodetectors with Picosecond Response-Times. *Appl. Phys. Lett.* **1984**, *44*, 450–452.

(19) Lee, C. H. *Picosecond Optoelectronic Devices*; Academic Press Inc.: Orlando, FL, 1984.

(20) Gao, J. B.; Fidler, A. F.; Klimov, V. I. Carrier Multiplication Detected Through Transient Photocurrent in Device-grade Films of Lead Selenide Quantum Dots. *Nat. Commun.* **2015**, *6*.818510.1038/ncomms9185

(21) Auston, D. H.; Lavallard, P.; Sol, N.; Kaplan, D. Amorphous-Silicon Photodetector for Picosecond Pulses. *Appl. Phys. Lett.* **1980**, *36*, 66–68.

(22) Yazdani, N.; Bozyigit, D.; Yarema, O.; Yarema, M.; Wood, V. Hole Mobility in Nanocrystal Solids as a Function of Constituent Nanocrystal Size. *J. Phys. Chem. Lett.* **2014**, *5*, 3522–3527.

(23) Nozik, A. J. Spectroscopy and Hot Electron Relaxation Dynamics in Semiconductor Quantum Wells and Quantum Dots. *Annu. Rev. Phys. Chem.* **2001**, *52*, 193–231.

(24) Sewall, S. L.; Cooney, R. R.; Anderson, K. E. H.; Dias, E. A.; Sagar, D. M.; Kambhampati, P. State-resolved Studies of Biexcitons

and Surface Trapping Dynamics in Semiconductor Quantum Dots. *J. Chem. Phys.* **2008**, *129*.08470110.1063/1.2971181
(25) Orenstein, J.; Kastner, M. Photocurrent Transient Spectroscopy - Measurement of the Density of Localized States in Alpha-As2se3. *Phys. Rev. Lett.* **1981**, *46*, 1421−1424.
(26) Tiedje, T.; Rose, A. A Physical Interpretation of Dispersive Transport in Disordered Semiconductors. *Solid State Commun.* **1981**, *37*, 49−52.
(27) Tiedje, T.; Cebulka, J. M.; Morel, D. L.; Abeles, B. Evidence for Exponential Band Tails in Amorphous-Silicon Hydride. *Phys. Rev. Lett.* **1981**, *46*, 1425−1428.
(28) Monroe, D. Hopping in Exponential Band Tails. *Phys. Rev. Lett.* **1985**, *54*, 146−149.
(29) Lee, C. H.; Yu, G.; Moses, D.; Heeger, A. J. Picosecond Transient Photoconductivity in Poly(P-Phenylenevinylene). *Phys. Rev. B: Condens. Matter Mater. Phys.* **1994**, *49*, 2396−2407.
(30) Moses, D.; Sinclair, M.; Heeger, A. J. Carrier Photogeneration and Mobility in Polydiacetylene - Fast Transient Photoconductivity. *Phys. Rev. Lett.* **1987**, *58*, 2710−2713.
(31) Moses, D. Charge Quantum Yield and Transient Transport-Properties of Anthracene and Amorphous Selenium. *Solid State Commun.* **1989**, *69*, 721−725.
(32) Lee, C. H.; Yu, G.; Moses, D.; Srdanov, V. I.; Wei, X.; Vardeny, Z. V. Transient and Steady-State Photoconductivity of a Solid C-60 Film. *Phys. Rev. B: Condens. Matter Mater. Phys.* **1993**, *48*, 8506−8509.
(33) Gao, J. B.; Jeong, S.; Lin, F.; Erslev, P. T.; Semonin, O. E.; Luther, J. M.; Beard, M. C. Improvement in Carrier Transport Properties by Mild thermal Annealing of PbS Quantum Dot Solar Cells. *Appl. Phys. Lett.* **2013**, *102*.04350610.1063/1.4789434
(34) Kang, M. S.; Sahu, A.; Norris, D. J.; Frisbie, C. D. Size- and Temperature-Dependent Charge Transport in PbSe Nanocrystal Thin Films. *Nano Lett.* **2011**, *11*, 3887−3892.
(35) Kaushik, A. R.; Lukose, B.; Clancy, P. The Role of Shape on Electronic Structure and Charge Transport in Faceted PbSe Nanocrystals. *ACS Nano* **2014**, *8*, 2302−2317.
(36) Gao, J. B.; Luther, J. M.; Semonin, O. E.; Ellingson, R. J.; Nozik, A. J.; Beard, M. C. Quantum Dot Size Dependent J-V Characteristics in Heterojunction ZnO/PbS Quantum Dot Solar Cells. *Nano Lett.* **2011**, *11*, 1002−1008.
(37) Gao, J. B.; Perkins, C. L.; Luther, J. M.; Hanna, M. C.; Chen, H. Y.; Semonin, O. E.; Nozik, A. J.; Ellingson, R. J.; Beard, M. C. n-Type Transition Metal Oxide as a Hole Extraction Layer in PbS Quantum Dot Solar Cells. *Nano Lett.* **2011**, *11*, 3263−3266.
(38) Tonouchi, M. Cutting-edge Terahertz Technology. *Nat. Photonics* **2007**, *1*, 97−105.
(39) Kim, S.; Lim, Y. T.; Soltesz, E. G.; De Grand, A. M.; Lee, J.; Nakayama, A.; Parker, J. A.; Mihaljevic, T.; Laurence, R. G.; Dor, D. M.; Cohn, L. H.; Bawendi, M. G.; Frangioni, J. V. Near-infrared Fluorescent Type II Quantum Dots for Sentinel Lymph Node Mapping. *Nat. Biotechnol.* **2004**, *22*, 93−97.

DOI: 10.1021/acsphotonics.6b00211
ACS Photonics 2016, 3, 1217−1222